

Chapter 8: Size Evolution of Annealed Silicon Nanoparticles

8.1. Introduction

Properties of nanoscale materials can differ vastly from the properties of the bulk.^[1] For silicon and other semiconductor materials, size reduction into the single nanometer range leads to novel optical properties as a result of quantum confinement of excitons.^[2] Decreasing the size of silicon nanoparticles to below 4 nm increases the band gap with a concomitant shift in excitonic emission to shorter wavelengths.

In addition to changes in the optical, magnetic, and physical properties, size reduction also affects the nature of the surface. Small particles cannot maintain the low energy surfaces found in the bulk; higher energy facets usually appear. The surface represents a greater fraction of the total particle and may influence some of the same properties that size affects.

For silicon, the surface can be either bare or, as is more typical, terminated with hydrogen or oxygen. Recently, a comparison between bare and hydrogen terminated particles indicated that the bare silicon nanoparticles with a diameter of 6 nm had a lower intensity of emission than hydrogen-terminated particles.^[3] Therefore, hydrogen termination appears to be important for excitonic emission from Si nanoparticles.

At larger surface curvature, hydrogen-terminated Si nanoparticles have been observed to have more silicon trihydride groups present.^[4] Hydrogen in this form is known to desorb at lower temperatures than the dihydride and monohydride form. Given the importance of hydrogen termination, the behavior of hydrogen desorption with particle size is of fundamental importance.

Holm and Roberts^[3] reported recently on hydrogen desorption from Si nanoparticles using an aerosol sizing method to compare particle size before and after thermal treatment of nanoparticles. The method utilized a low-pressure plasma to synthesize a broad distribution of nanoparticles starting with silane as a precursor. A differential mobility analyzer (DMA) was used subsequently to select a narrow slice of the distribution centered at 6 nm. The size-selected distribution was then passed through a furnace, and the resulting particle size distribution was measured in a second DMA. The measured particle size was observed to change a total of ~ 0.32 nm over three temperature ranges: low ($20^{\circ}\text{C} - 300^{\circ}\text{C}$), medium ($300^{\circ}\text{C} - 400^{\circ}\text{C}$), and high ($600^{\circ}\text{C} - 700^{\circ}\text{C}$). The largest diameter decreased in the medium temperature range (i.e., 0.21 nm) whereas smaller diameter decreases were observed for the low (i.e., 0.07 nm) and high (0.04 nm) temperature ranges. Comparing the size changes with IR and ToF-SIMS data revealed that these temperature ranges corresponded to hydrogen desorption from silicon trihydride, dihydride, and monohydride, respectively.

The temperature dependence of the observed size reduction should be different for smaller particles because of differences in hydrogen surface coverage due to curvature. In the present study, we focus on nanoparticles in the 1 to 4 nm range to investigate the size dependence of hydrogen desorption with a tandem arrangement of

two nano-RDMAs appropriate for the lower size regime. We adopted the tandem configuration because it offers several advantages: (1) it reduces significantly the number of particles thereby preventing agglomeration; (2) it narrows the size distribution so that the observed size change can be attributed to a particular particle size; and (3) it prevents any unreacted precursor from contributing to particle growth in the furnace.

8.2. Experimental Description

The dependence of hydrogen desorption on particle size was studied using an atmospheric-pressure direct current microdischarge (MHCD),^[5] shown schematically in figure. 8.1. The discharge is maintained between a cathode (stainless steel capillary tube, I. D. $\approx 180 \mu\text{m}$) and an anode (stainless steel tube, O. D. $\approx 3 \text{ mm}$). The electrode assembly is enclosed in a glass tube (O. D. $\approx 12 \text{ mm}$) using standard Swagelok and UltraTorr fittings. An ultrahigh purity (UHP) argon/silane gas mixture flows through the capillary at a flow rate of 150 standard cubic centimeters per minute (sccm). In the afterglow portion of the microplasma between the two metal electrodes, a second UHP argon stream is added at a flow rate of 450 sccm to dilute the particles. This combined stream enters the first nano-Radial DMA (nano-RDMA),^[6] which is used either to characterize the particle size distribution or to select a fraction of particles for subsequent annealing. For particle sizing, the aerosol outlet flow of the nano-RDMA is directed to a home-built faraday cup electrometer sensitive to $\pm 1 \text{ fA}$. This permits determination of the particle size distribution originating in the microdischarge. The nano-RDMA is operated in stepping mode using a computer to control the voltage applied to the device. A two-second delay is used to stabilize the voltage before recording the average electrometer reading over one second. Once the size distribution from the microplasma is

determined, a constant voltage is applied to the first nano-RDMA to select a portion of the distribution around the maximum of the initial distribution. The peak position of the size distribution could be varied by changing the silane concentration introduced into the microplasma. The aerosol outlet of the nano-RDMA is connected to a thermal processing stage, consisting of an Inconel tube in a temperature-controlled furnace. After the thermal processing stage, the aerosol flow is actively cooled and directed to a second nano-RDMA for postannealing size analysis that is performed as described for the first nano-RDMA.

Measured particle size distributions were fit with a lognormal distribution using MatLab with concentration, geometric mean mobility diameter, and geometric standard deviation as the fitting parameters. While theoretical calculations have shown different structures for the hydrogenated and dehydrogenated clusters,^[7] the mobility diameters calculated here are based on the assumption of a spherical particle.

8.3. Results and Discussion

The MHCD produces a particle size distribution that is well-fit by a log normal distribution. A representative particle scan is shown in figure 8.2, which was recorded after the MHCD with the first nano-RDMA. Although not shown, the geometric mean mobility diameter could be shifted to larger sizes by increasing precursor concentration. Average particle size increases were accompanied by broadening of the distribution. For all precursor concentrations, the standard geometric deviations measured were less than reported literature values given the higher resolution of our nano-RDMA as compared to device intended for larger size regimes.^[5] The narrow size distribution of the as produced

nanoparticles for silane concentrations of 1 and 2 ppm required selecting the peak of the distribution to complete further experimentation.

A size distribution selected by fixing the voltage in the first nano-RDMA could be measured with the second nano-RDMA. A comparison between the two distributions is also made in figure 8.2. It is important to note that the distribution measured in the second nano-RDMA indicates a lower particle density, consistent with expected diffusion losses inside the processing stage. Increasing the furnace temperature decreases further the measured particle concentrations due to thermophoretic losses upon cooling the aerosol prior to the second nano-RDMA. Such losses are particularly severe for smaller particles given the lower initial particle densities.

For the largest particle size studied (i.e., 3.1 nm), the mean mobility data are shown in figure 8.3 as a function of the annealing temperature. The observed overall size reduction (i.e., 0.35 nm) occurred over three temperature ranges. The size reduction was 0.13 nm between 25°C and 300°C, followed by a 0.16 nm decrease in size between 300°C and 400°C, and 0.06 nm over a third temperature range of 400°C and 600°C. The proportion of the measured size reduction for each temperature range is different for particles with a smaller initial size (i.e., 2.7 nm), as depicted in figure 8.4. A greater portion of the overall size change occurs below 300°C (i.e., 0.23 nm), yet the overall size change is approximately the same (i.e., 0.35 nm). Beyond 400°C, the measured particle size changes only in a minor way (i.e., 0.02 nm). The size reduction for even smaller particles (i.e., 1.7 and 1.3 nm) is found to be quite different (figures 8.5A and 8.5B). The overall size reduction (i.e., 0.25 and 0.11 nm) was less than what was observed for the

larger particles and occurred almost completely in the low temperature range (i.e., 20°C and 300°C).

To examine the observed size change due to thermal annealing on a more consistent basis requires converting the data to a slightly different format. The smallest measured diameter is assumed to be the bare silicon nanoparticle and is subtracted from each measured size, as shown in figure 8.6. In this format, the change in size reduction behavior for different initial diameter particles as a function of temperature is demonstrated directly. In addition to the data collected in this experiment, the previously reported data are plotted for comparison.^[3]

The size change for the two largest diameters studied (i.e., 3.1 and 2.7 nm) proceeded similar to that reported for 6 nm particles.^[3] The overall size reduction of 0.35 nm measured in this report is very similar to the 0.32 nm found. For the largest diameter measured (i.e., 3.1 nm), the overall size change proceeded over three similar temperature ranges.

Yet, the proportion of the change that was observed over each temperature range was different. The size reduction of 0.1 nm between 25°C and 300°C is larger than that reported for the 6 nm particle.^[3] As before, a second region is observed between 300°C and 400°C over which a decrease in size of 0.15 nm is observed, a size change that is smaller than reported for the 6 nm particle. The final size change occurs at a lower temperature than previously reported but is similar in magnitude. Similar behavior is observed for particles with an initial diameter of 2.7 nm, but a larger portion of the overall size decrease occurred in the low temperature range.

Based on similarities in synthesis, these results are interpreted in terms of hydrogen evolution. For the low temperature range, the observed changes in diameter would be due to hydrogen desorption from silicon trihydride species. As the surface curvature increases (i.e., decreasing particle size), more of the surface would be covered in silicon tri-hydride groups. Therefore, smaller particles would have a greater portion of the observed size change in the low temperature range.

In the medium temperature range, the size change is attributed to silicon dihydride evolution. The opposite trend would be expected in this range as more silicon trihydride termination would result in less silicon dihydride coverage. Correspondingly, the portion of the diameter change increases with increasing size in this temperature range.

The difference in size reduction behavior becomes more drastic for the two smallest initial sizes measured. The overall diameter change is less than that observed for the larger particles, indicating most likely incomplete hydrogen surface coverage. The incomplete surface coverage could be due to the conditions present in the MHCD or due to an increase in the surface energy at such high surface curvatures.

To determine whether the measurements were of a kinetically limited process, the furnaces were operated at different temperatures (data not shown). It was found that the measured particle size was identical when only one furnace is set to 400°C (i.e., second furnace at 20°C) and when both furnaces were at 400°C. Similar measurements at other combinations of furnace temperatures confirmed that the size measurements were not of kinetically limited process.

8.4. Summary

The size evolution of silicon nanoparticles due to thermal annealing depends on the initial particle size. Three different temperature ranges were observed over which the particle size changed that were consistent with hydrogen desorption found in previous studies. Smaller particles evolved to the bare particle size at lower temperatures than larger particles. The data are consistent with smaller particles containing more silicon trihydride than larger particles. These measurements were not kinetically limited as increasing the residence time in the furnace did not affect the resulting particle size.

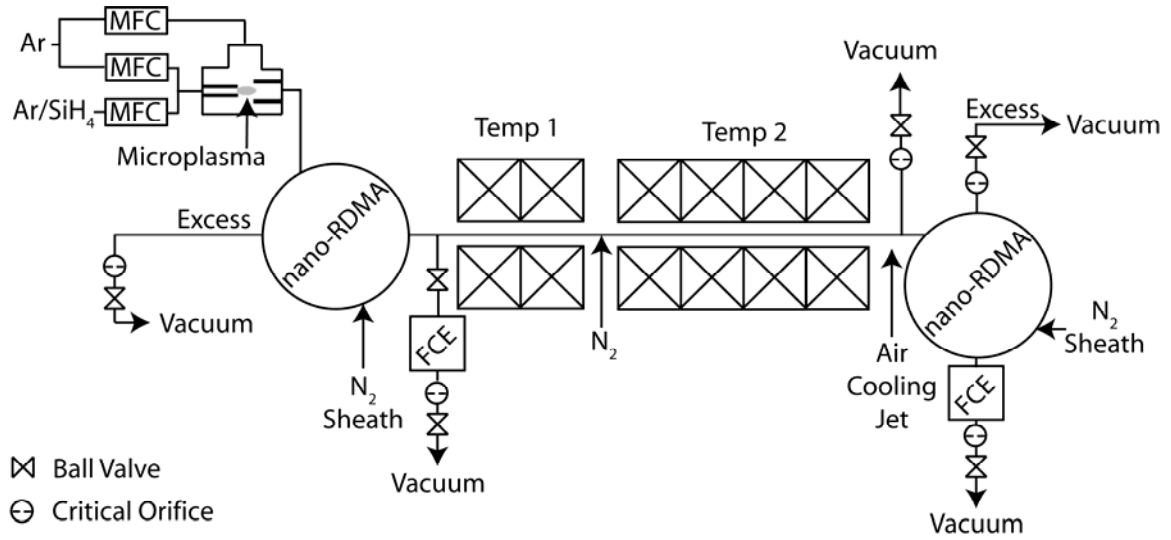


Figure 8.1. Schematic of Tandem DMA Sintering Arrangement.

Schematic of the microplasma and the tandem differential mobility analyzer arrangement used to sinter silicon nanoparticles. The furnace temperatures are independently controllable. The air cooling jet was used to maintain the temperature of the gas line at room temperature.

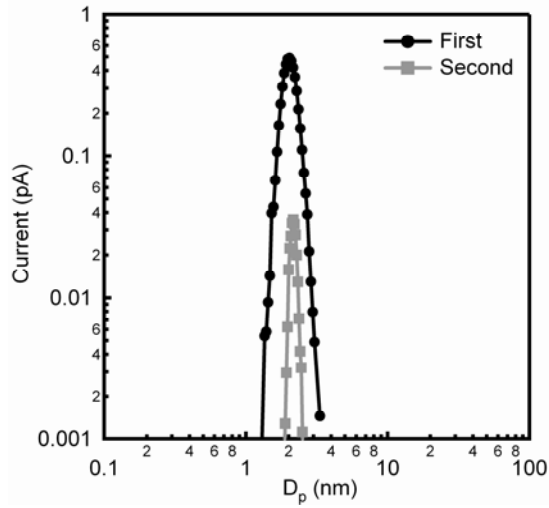


Figure 8.2. Size Distribution of First and Second nano-RDMA.

Comparison of the particle size distributions measured after the first and second nano-RDMA. The silane concentration introduced into the plasma was 2 ppm.

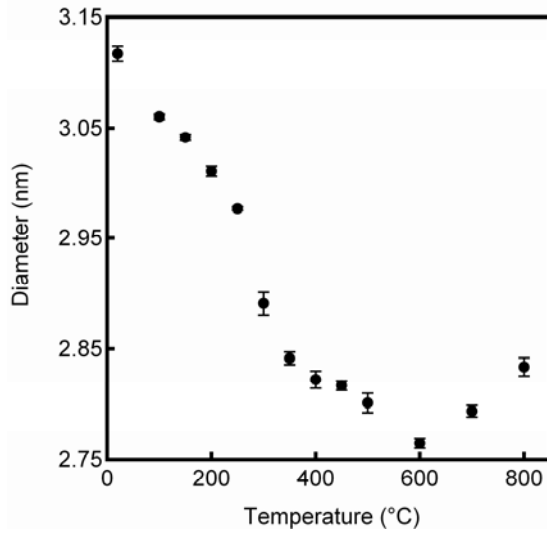


Figure 8.3. Size Variation of 3.1 nm Silicon Nanoparticles with Temperature.

Particle size measured at different temperatures for an initial silane concentration of 4 ppm in the microplasma.

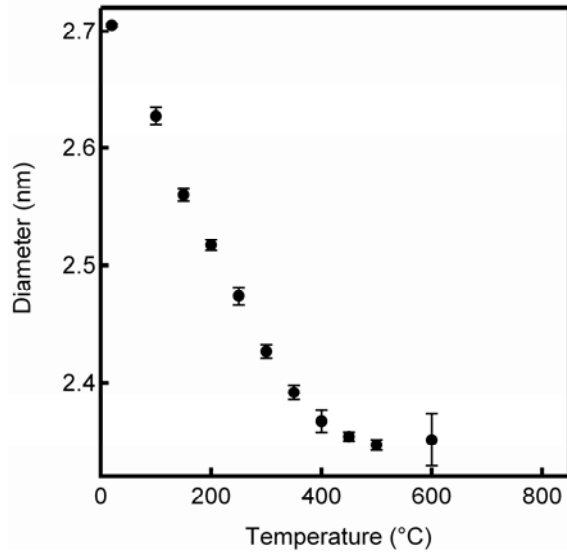


Figure 8.4. Size Variation of 2.7 nm Silicon Nanoparticles with Temperature.

Particle size measured at different temperatures for an initial silane concentration of 3 ppm in the microplasma.

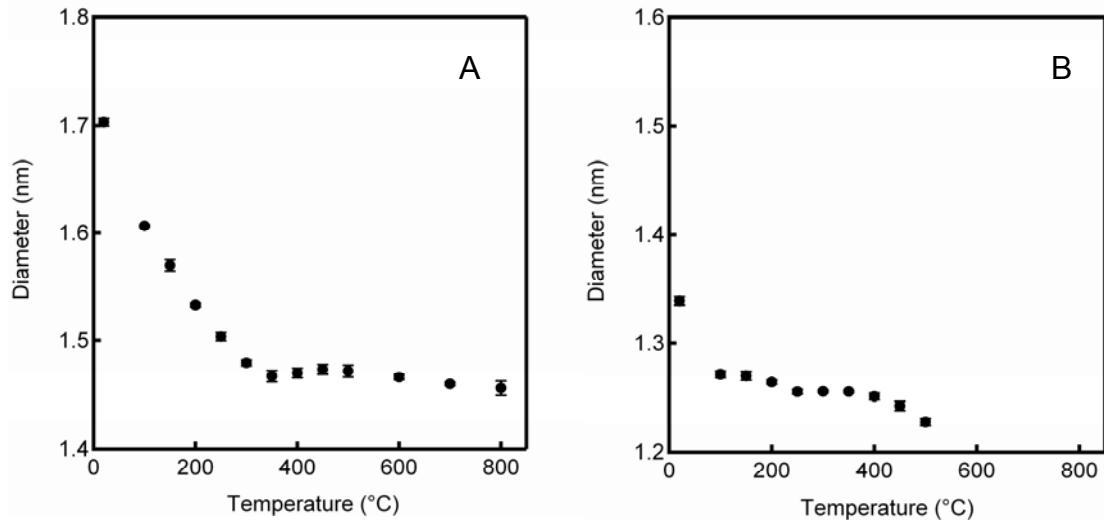


Figure 8.5. Size Variation of 1.7 and 1.3 nm Silicon Nanoparticles with Temperature.

Particle size measured at different temperatures for an initial silane concentration of 2 ppm (A) and 1 ppm (B) in the microplasma.

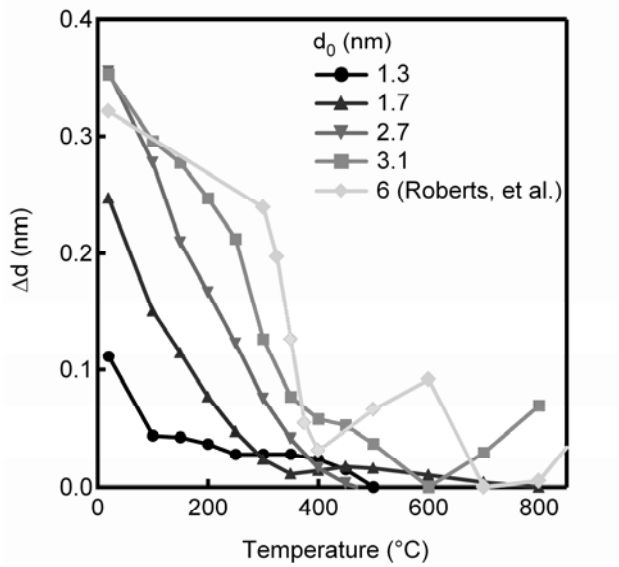


Figure 8.6. Comparison of Size Variation with Temperature.

Measured diameter difference with temperature between minimum particle size for silane precursor concentrations of 1, 2, 3, and 4 ppm. Data from a previous report is included for comparison.^[3]

References

1. G. Schmid, *Chemical Reviews*, **92**, 1709, 1992.
2. A. Cullis, and L. Canham, *Nature*, **353**, 335, 1991.
3. J. Holm, and J. Roberts, *Journal of the American Chemical Society*, **129**, 2496, 2007.
4. N. Salivati, and J. Ekerdt, *Surface Science*, **603**, 1121, 2009.
5. R. Sankaran, D. Holunga, R. Flagan, and K. Giapis, *Nano Letters*, **5**, 537, 2005.
6. N. Brunelli, R. Flagan, and K. Giapis, *Aerosol Science and Technology*, **43**, 53, 2009.
7. A. Barnard, and P. Zapol, *The Journal of Chemical Physics*, **121**, 4276, 2004.